Journal of Asian Concrete Federation
Vol. 2, No. 1, pp. 56-66, June 2016
ISSN 2465-7964 / eISSN 2465-7972
http://dx.doi.org/10.18702/acf.2016.06.2.1.56

Effect of perpendicular beams on failure of beam-column knee joints with mechanical anchorages by 3D RBSM

Liyanto Eddy*, Koji Matsumoto and Kohei Nagai

(Received: January 31, 2016; Accepted: May 16, 2016; Published online: July 05, 2016)

Abstract: When mechanical anchorages are placed near the surface of a beam-column knee joint, anchorage failure may occur because of local stresses from anchorage plates. Perpendicular beams placed on both sides of the joint can be a way to avoid the occurrence of this failure. In this study, a meso-scale discrete analysis using 3D RBSM is conducted to investigate the effect of perpendicular beams on the behavior of a beam-column knee joint with mechanical anchorages and their effect on failure mode. By studying the internal stresses and cracks in a beam-column knee joint with mechanical anchorages, perpendicular beams can improve its performance in terms of loading capacity and failure behavior. Perpendicular beams are known to have two effects. The perpendicular beams increase bond performance along the development length of anchorages and resist the opening of the diagonal cracks. It has the same failure mode as in the case without perpendicular beams which is an anchorage failure, but the occurrence of the anchorage failure is delayed in this case. It is also inferred by simulation that the effective length of the perpendicular beams is determined by approximately 45 degrees inclination to the longitudinal beam, measured from the original position of anchorage plates.

Keywords: beam-column knee joints, mechanical anchorages, meso-scale analysis, 3D RBSM.

1. Introduction

Reinforcement congestion in beam-column joints leads to increased compaction time and more difficulty in ensuring proper concrete compaction. Mechanical anchorage is one way to reduce this congestion. In this study, the mechanical anchorage is used to refer to headed reinforcement. Because it has an anchorage plate at the end of the anchorage, the anchorage length can be shorter than a conventional hooked bar and the anchorage detail becomes simpler as shown in Fig. 1. However, if mechanical anchorages are placed near the surface of a beam-column knee joint, anchorage failure may occur because of local stresses from anchorage plates when it is loaded by a moment that tends to close the beam-column joint [1-3]. In addition, this failure leads to a dramatic decrease in the loading capacity of a beam-column knee joint. Here, the anchorage failure is defined as a joint failure initiated by the local stresses and cracks from anchorage plates. Perpendicular beams, which are placed on both sides of a joint, can be a way to avoid the occurrence of this anchorage failure. Previous experimental work [4] has shown that in case of a beam-column exterior joint with mechanical anchorages, these perpendicular beams can improve the performance. However, the effect of perpendicular beams on the macroscopic behavior, in case of a beam-column knee-joint with mechanical anchorages has not been investigated.

Fig. 1 – Mechanical anchorage: headed reinforcement

Numerical simulation can be a beneficial tool for understanding the macroscopic behavior because internal stresses and internal crack conditions can be investigated. Meanwhile, experimental program will take time and is inefficient. A numerical simulation should satisfy the following three requirements in this study. Firstly, it is a 3D simulation where the reinforcement arrangement can be accurately represented by modelling the 3D shape of reinforcement including its ribs. Secondly, it is a meso-scale simulation, at a size range of 10-20 mm, so that the local failure can be precisely predicted

Corresponding author Liyanto Eddy is Postdoctoral Research Fellow of Institute of Industrial Science, The University of Tokyo, Japan.
Koji Matsumoto is a Project Assistant Professor, Institute of Industrial Science, The University of Tokyo, Japan.
Kohei Nagai is an Associate Professor, Institute of Industrial Science, The University of Tokyo, Japan.

by checking for discontinuous deformation of the concrete and the interaction between concrete and reinforcing bars at this scale. Finally, cracks can be simulated directly. Thus, a meso-scale analysis using 3D discrete element analysis called 3D Rigid Body Spring Model (RBSM) is an appropriate approach. In previous researches with RBSM [5-9], 2D RBSM was conducted to investigate the behavior of reinforced concrete members as well as that of pre-stressed concrete members. Furthermore, 3D RBSM was used to simulate fiber-reinforced cement composites [10-11] and shrinkage phenomena [12]. In our research group, 3D RBSM has been used to study the behavior of reinforced concrete members by directly modelling the shape of the reinforcement in 3D, including its ribs [13-14]. In detail, there are several merits of 3D RBSM in this study of the beam-column knee joints with mechanical anchorages. It can reveal the local responses of concrete and a mechanical anchorage including its mechanical plate and ribs and their interactions with cracking in 3D. Using such simulation, the effect of reinforcement anchoring in a multi-directional arrangement in a beam-column knee joint can be investigated by studying the three dimensional stress transfer mechanism. In addition, since the results of simulation can provide a step by step understanding of the internal stresses and internal crack conditions, it is possible to investigate how the stresses initially developed from local scale, affect the macroscopic response after several steps of loading. It is called the failure process.

There are two ultimate aims of this research. The first is to investigate the effect of perpendicular beams on the macroscopic behavior of beam-column knee joints with mechanical anchorages through the study of internal stresses and internal cracks using numerical simulations. Meanwhile, the second is to understand the failure mode of beam-column knee joints with mechanical anchorages when perpendicular beams are added on both sides of beam-column knee joints. A beam-column knee joint without perpendicular beams will also be simulated as a control case and, in this case, the simulation results are compared with the experimental results.

2. Numerical method and constitutive models

2.1 Numerical method

Simulations are carried out by 3D RBSM, as proposed by Kawai et al. [15]. A 3D reinforced concrete model is formed from a mesh of rigid bodies. Each rigid body has six degrees of freedom, consisting of three translational degrees of freedom and three rotational degrees of freedom around certain points within its interior. Each rigid body is connected to other rigid bodies by two shear springs and one normal spring as illustrated in Fig. 2. Concrete and steel elements are used to model a reinforced concrete member in 3D. The mesh arrangement in the model in RBSM is important because the crack propagation in reinforced concrete is one of the most important factors affecting its behavior. Random geometry, with the help of a Voronoi diagram, is used for element meshing to prevent cracks from propagating in a non-arbitrary direction. Concrete elements are modelled with a size of approximately 10×10×10 ~ 20×20×20 mm, which is similar to the aggregate size, in order to ensure a cracking pattern similar to actual concrete. It is well known that, in normal concrete, the zig-zag path of crack propagation is affected by the aggregate size and its location. Thus, in order to replicate and consider the effect of aggregate on this real cracking pattern, random element generation, approximately 10 ~ 20 mm in size, is chosen. The geometry of steel elements is modelled accurately, with full 3D modelling of the reinforcing bar arrangement including its ribs, in order to properly account for the interlocking between reinforcement and concrete. The meso-scale mesh arrangement used for concrete and steel in this study is illustrated in Fig. 3. The properties of springs are determined such that the elements, when combined together, are able to accurately predict the response determined in laboratory scale material tests. The simulation system developed by Nagai et al. [16] is used.

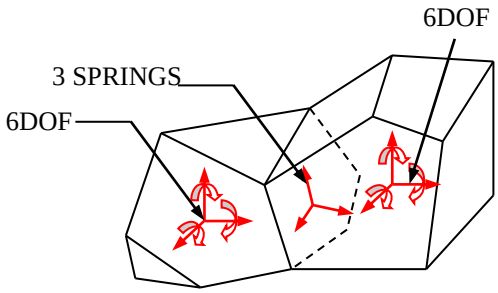

Fig. 2 – 3D RBSM mechanical model

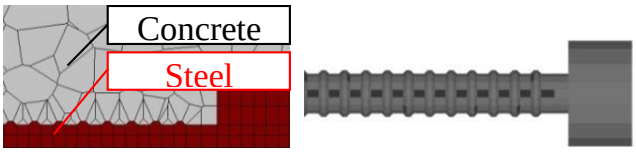

(a) Cross section (b) 3D Model re-bar

Fig. 3 – Mesh arrangement for concrete and re-bar

2.2 Constitutive models of elements

Concrete and steel elements are used to represent the behavior of reinforced concrete in this study.

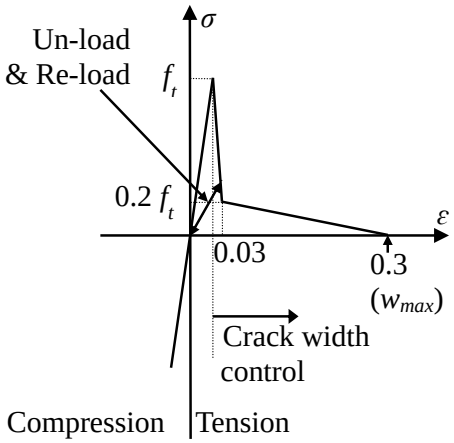

(a) Normal spring of concrete

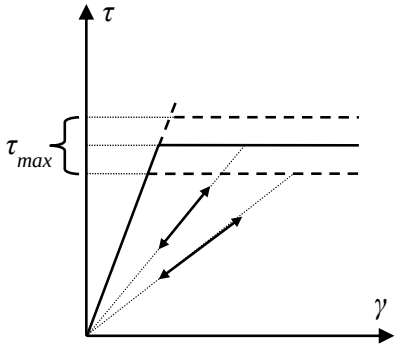

(b) Shear spring of concrete

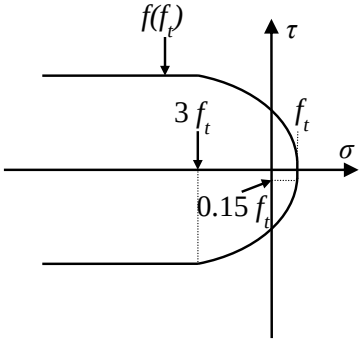

(c) τ_{max} criterion of concrete

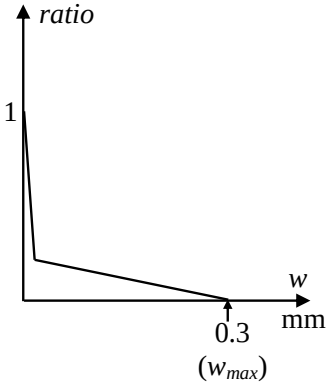

(d) Shear reduction factor

Fig. 4 – Constitutive models of concrete

(1) Concrete elements

As mentioned above, the shape of concrete elements is determined randomly using a Voronoi diagram. However, the elements near steel elements are constructed manually in order to follow the actual 3D geometry of the reinforcing bars. Random element generation is thought to lead to accurate replication of the concrete fracture process. The constitutive models for the normal and shear springs of concrete elements are presented in Fig. 4. In the compression zone, the normal springs of the concrete elements behave elastically, since compressive failure is not allowed at the meso scale. A crack is defined when the tensile stress of normal springs exceeds the tensile strength of the concrete elements (f_{telem}). After the tensile strength (f_{telem}) is exceeded, the tensile stress of the normal spring is assumed to decrease bi-linearly depending on the crack width between two rigid bodies. The maximum crack width (w_{max}) is assumed to be 0.3 mm as shown in Fig. 4(a). On the other hand, an elasto-plastic behavior is assumed for the shear spring of the concrete elements, as shown in Fig. 4(b), where the maximum value of the shear stress is calculated based on Eq. (1) and presented in Fig. 4(c). Here, the tensile strength of concrete elements is same as the tensile strength of concrete material.

$$\tau_{max} = \pm(1.6 f_{telem}^{2}(-\sigma+f_{telem})^{0.4}+0.15 f_{telem}) \text{ if } (\sigma \geq 3 f_{telem})$$
$$\tau_{max} = \pm(1.6 f_{telem}^{2}(4 f_{telem})^{0.4}+0.15 f_{telem}) \text{ if } (\sigma < 3 f_{telem}) \quad (1)$$

where τ_{max} is maximum value of shear stress (MPa), f_{telem} is tensile strength of concrete elements (MPa), and σ is normal stress of concrete elements (MPa).

When a fracture occurs in the normal springs, the calculated shear stress is reduced according to the reduction in normal stress. As a result, the shear springs cannot carry the shear stress when the crack width of the normal spring exceeds w_{max} as shown in Fig. 4(d).

(2) Steel elements

The geometry of steel elements is modelled in an accurate manner to properly account for the interlocking between concrete and a reinforcing bar as illustrated in Fig. 3. The normal springs of steel elements are modelled based on the stress-strain relationship of a steel bar proposed by Shima et al. [17]. The stress-strain relationship used for the normal springs is represented by Eq. (2). Meanwhile, the shear springs used for the steel elements are assumed to be perfectly elastic.

$$\sigma_s = E_s \varepsilon_s \quad \text{if } (\varepsilon_s < \varepsilon_y)$$
$$\sigma_s = f_y \quad \text{if } (\varepsilon_y < \varepsilon_s < \varepsilon_{sh})$$
$$\sigma_s = f_y+(1-e^{((\varepsilon sh-\varepsilon s)/k)})(1.01 f_u-f_y) \quad \text{if } (\varepsilon_s > \varepsilon_{sh}) \quad (2)$$

Table 1 – Detail of numerical models

Case	Parameter	Material properties of concrete			Number of elements	Maximum load	
		Compression	Tension	Elasticity		Exp.	Ana.
		f'_c (MPa)	f_t (MPa)	E_c (MPa)		(kN)	(kN)
AL2	Without perpendicular beams	30.8	2.43	27,900	756,638	94.5	85.0
AL2PER	With perpendicular beams	30.8	2.43	27,900	953,166	-	109.45
AL2PER-E	With perpendicular beams and elastic reinforcement	30.8	2.43	27,900	953,166	-	127.38

Table 2 – Properties for AL2 by Tasai et al. [3]

Flexural strength of the beam	196.5 kN.m
Story shear at beam flexural yielding	111.5 kN
Flexural strength of the column	194.2 kN.m
Story shear at column flexural yielding	114.2 kN
Joint shear strength*	445 kN

Note: Joint shear strength is calculated by $V_{ju}=k_j.\phi.F_j.b_j.D_j$ [18], where V_{ju}=joint shear strength (kN), k_j=0.4, ϕ=0.85, $F_j=0.8(f'_c)^{0.7}$, f'_c=compressive strength of concrete (MPa), D_j=column depth (mm), b_j=effective width of beam-column joint (mm).

where, $k = 0.032(400/f_y)^{1/3}$, σ_s is steel stress (MPa), ε_s is steel strain, f_y is yield strength (MPa), f_u is tensile strength (MPa), ε_{sh} is initial strain hardening, assumed to be 1.5%.

(3) Concrete-steel interface

At the concrete-steel interface, the constitutive models of the normal springs and the shear springs have the same behavior as those of concrete elements as shown in Fig. 4(a). However, in order to consider the concrete-steel interface as a weak region, the tensile strength of the interface element is assumed to be half that of concrete elements.

3. Detail of numerical simulations

3.1 Numerical models

Three numerical models are considered in this study. The simulation cases are listed in Table 1. One experimental specimen is selected from among those used in experiments by Tasai et al. [3]. This model is implemented to clarify the occurrence of anchorage failure in a beam-column knee joint with mechanical anchorages. The notation in this model is the same as that used for the original experimental specimen which is named by AL2. Further, one numerical model is used to investigate the effect of perpendicular beams on the behavior of the beam-column knee joint with mechanical anchorages in which perpendicular beams are added on both sides of the earlier case (AL2). This model is named by AL2PER. In addition, in order to understand the failure mode of joint part of the model AL2PER, one additional numerical model, named AL2PER-E is used in which the yield strength of the longitudinal reinforcement in the beam is assumed to remain elastic to avoid the flexural failure.

3.2 Geometry of numerical models

Figure 5 shows the geometries of the numerical models. AL2 has the same dimensions as those in the experimental specimen. For the comparison, details of the original experimental specimen are included in Fig. 6. Table 2 shows the properties for AL2 in terms of flexural capacity of the beam and column and joint shear strength. In AL2PER and AL2PER-E, the dimensions are basically similar to AL2, but additional perpendicular beams are placed on both sides of the joint. The perpendicular beams are assumed to be 480 mm in width, 400 mm in height, and 400 mm in length.

The reinforcement arrangements in the numerical models also match those of the experimental specimen, with deformed bars of 19 mm and 22 mm used as the main column and beam reinforcement, respectively. Meanwhile, in order to reduce the computational time, the stirrups of the beam and column are modelled as plain bars of 10 mm.

Table 3 – Material properties of reinforcement

Re-bars	Function	Yield strength (MPa)	Modulus of elasticity (MPa)
D22	Main reinforcement of column	377	183,000
D19	Main reinforcement of beam	435	184,000
D10	Beam and column stirrups	363	203,000

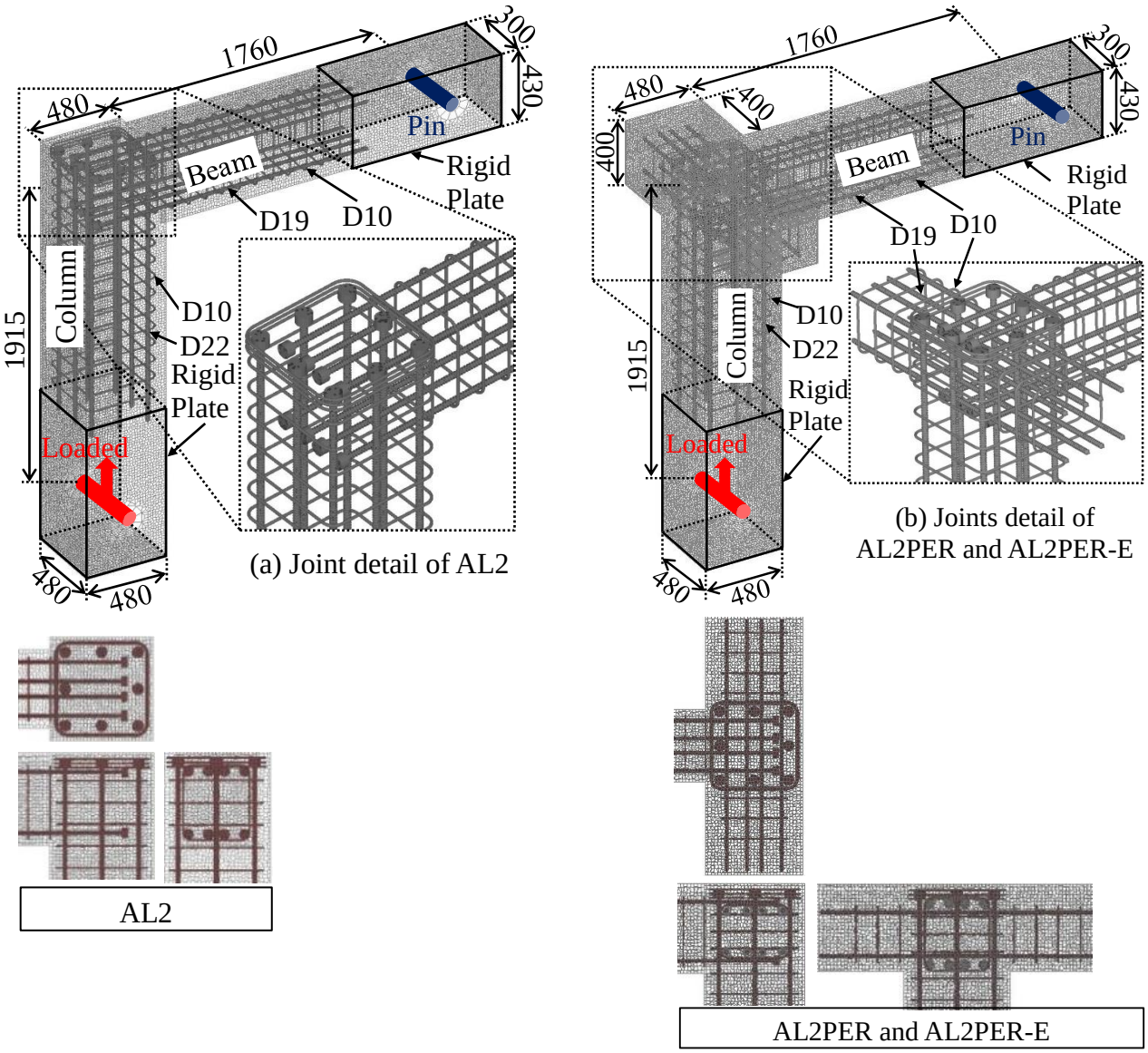

Fig. 5 – Geometries and boundary conditions of numerical models (unit: mm)

In AL2PER and AL2PER-E, the reinforcement arrangements in the perpendicular beams are assumed to be the same as those in the main beam. The material properties of the reinforcement in each model are shown in Table 3.

3.3 Boundary conditions

Figure 5 also shows the boundary conditions of the numerical models. For comparison, details of experimental arrangement are shown in Fig. 7. Rigid steel plates are modelled at the ends of main beam as well as main column to model rigidity such that deformation of the plates is prevented. Pin elements are introduced inside the steel plates in order to model the hinge condition in the experimental arrangement. Only compressive stresses act between pins and plates. Friction is not allowed between the pins and the plates by setting the stiffness of shear springs to zero between these two elements.

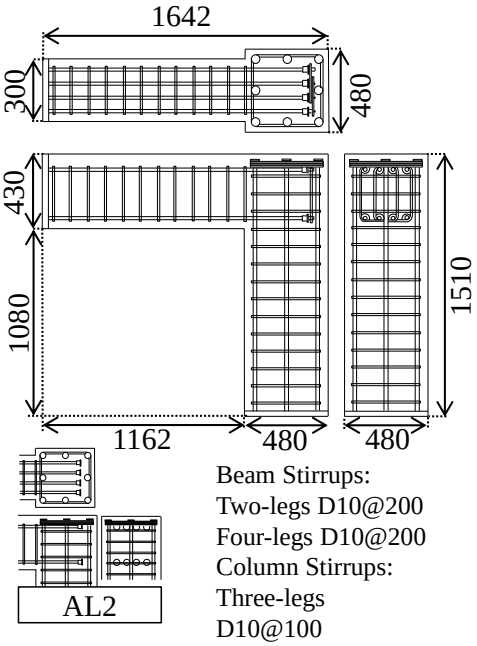

Fig. 6 – Experimental specimen by Tasai et al. [3] (unit: mm)

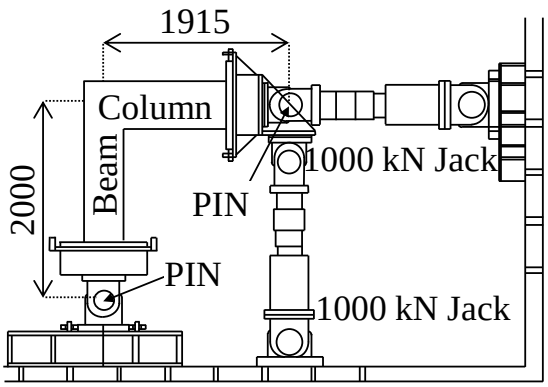

Fig. 7 – Experimental arrangement by Tasai et al. [3] (unit: mm)

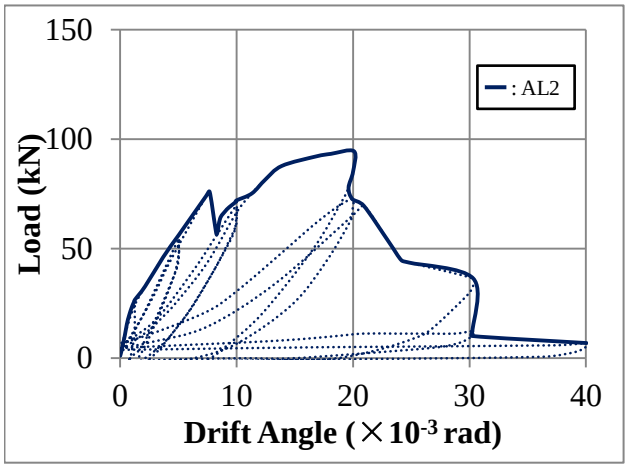

(a) Experimental result by Tasai et al. [3]

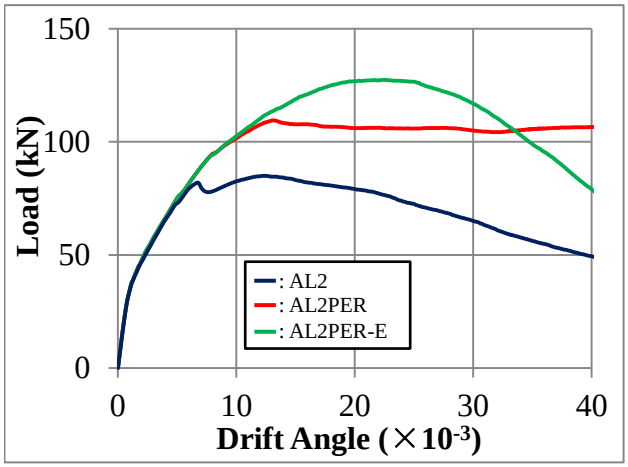

(b) Simulation results

Fig. 8 – Load-displacement relationships

Since anchorage failure occurs due to a moment that tends to close the joint, this loading condition is of main interest in this study. Cyclic load applied in the experiment is not modelled in this simulation. In order to represent the moment that tends to close the beam-column joint, push load is applied to the pin in the rigid plate located at the end of the column, while the pin in the rigid plate located at the end of the beam is fixed. Monotonically increasing displacement is applied in the simulation. This displacement is increased by 0.1 mm at each loading step. A total of 800 steps of displacement-loading is applied in the simulation.

4. Numerical simulation results and discussion

4.1 Load-displacement relationships

The load-displacement relationships for AL2, both simulation and experimental observation, are shown in Fig. 8. The load-displacement relationships for AL2PER and AL2PER-E are also included in Fig. 8(b). Maximum loads are included in Table 1. The load is defined as the load applied on the pin in the rigid plate located at the end of the column, while the displacement is calculated based on the drift angle. In AL2, the maximum load obtained by the simulation result is comparable to that observed in the experimental specimen. The peak load obtained from the simulation results is only 5% less compared to the experimental results. Thus the simulated maximum load is in good agreement with the experimental result.

It is predicted in the simulations that the maximum load in AL2PER (perpendicular beams) is 28.8% higher than AL2 (without perpendicular beams), while AL2PER-E (perpendicular beams and elastic reinforcement) exhibits the highest maximum load, 49.9% higher than AL2 (without perpendicular beams). It means that the perpendicular beams increase the loading capacity of a beam-column knee joint with mechanical anchorages. After exceeding the maximum load, the behavior varies depending on the failure mode of the beam-column joint. It is observed in the experiment that an anchorage failure occurs in AL2 and, furthermore, the load decreases dramatically once the maximum load is exceeded. The same behavior is predicted by the simulation. In AL2PER, the simulation predicts that the load does not decrease after exceeding the maximum load, indicating a flexural failure. It is also confirmed by AL2PER-E that the loading capacity can increase more than AL2PER because of the increased yield strength of the longitudinal reinforcement in the beam which indicates the yielding of the longitudinal reinforcement in the beam in AL2PER. In AL2PER-E, the simulation result shows that the load decreases significantly after exceeding the maximum load. It can be concluded that the flexural failure will not occur in this case. By studying the internal stresses and cracks in the simulation results, the causes of the change in the failure mode in AL2PER and AL2PER-E are investigated.

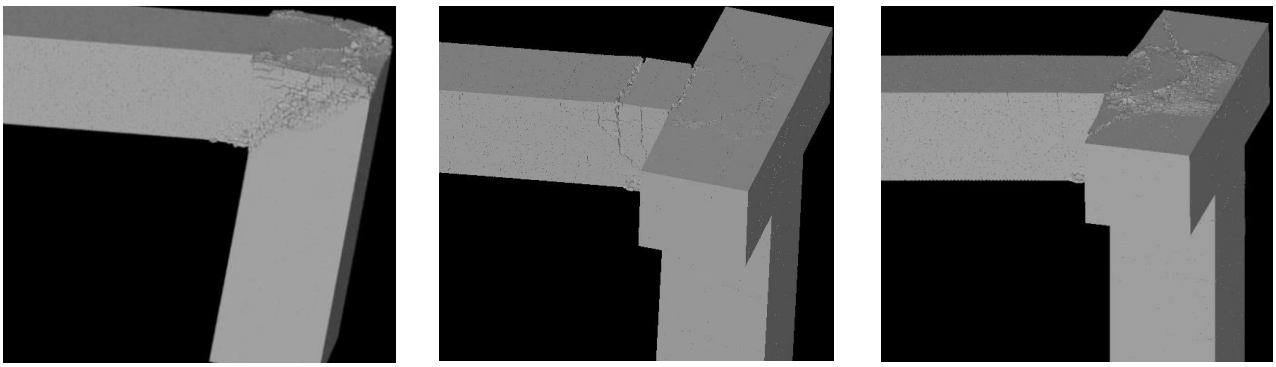

(a) AL2 (b) AL2PER (c) AL2PER-E

Fig. 9 – Surface cracks in 3D (deformation×3)

4.2 Surface cracks

A 3D representation of the surface cracks in AL2 (anchorage failure), AL2PER (flexural failure), and AL2PER-E (anchorage failure) is shown in Fig. 9. Figure 10 shows the crack patterns for all simulation models in comparison with the photos of AL2 obtained by the experiment after the failure. In AL2, the simulation matches the observed crack patterns well as shown in Fig. 10(a). Diagonal cracks, propagating from the anchorage plates of the top longitudinal reinforcement in the beam to the inner corner of the beam-column joint (1a) and from the anchorage plates of the middle longitudinal reinforcement in the column to the inner corner of the beam-column joint (1b), occur on both sides of AL2. The damage at the top surface in the simulation matches that of the experimental specimen which indicates an anchorage failure in this case (2). However, the concrete spalling in the experimental specimen is not well simulated.

In AL2PER, Fig. 10(b) shows that cracks spread out to the perpendicular beams (2). The flexural cracks in this case are wider than in AL2 (3) which indicates the flexural failure in the beam-column joint. In AL2PER-E, Fig. 10(c) shows that the damage at the top surface of the joint occurs, which indicates the anchorage failure in this case (2). In addition, the width of flexural cracks in AL2PER-E is smaller than in AL2PER. This confirms that the flexural failure doesn't occur in AL2PER-E. It can be concluded that AL2PER-E has the same failure behavior as AL2. In addition, mechanical anchorages of the column reinforcement don't affect these macroscopic failures of the joints.

(a) AL2

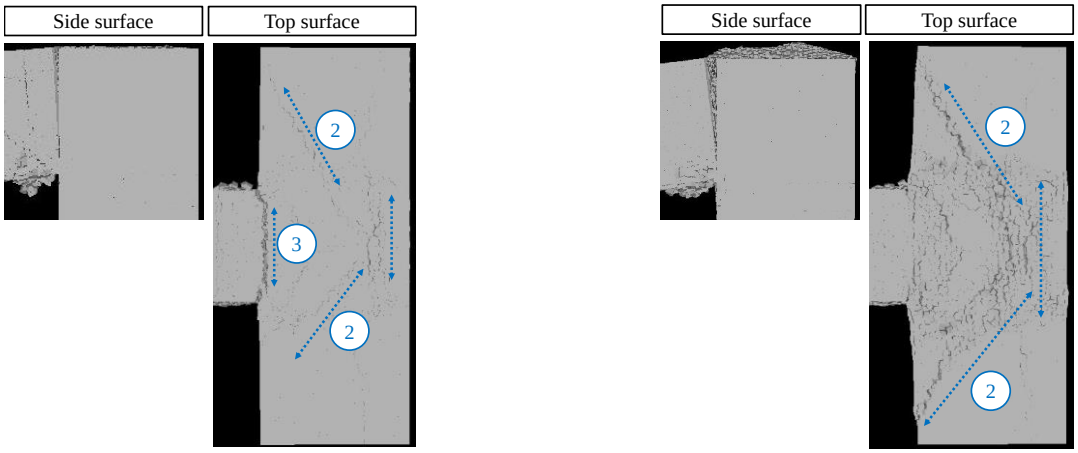

(b) Simulation for AL2PER (deformation×3) (c) Simulation for AL2PER-E (deformation×3)

Fig. 10 – Surface cracks

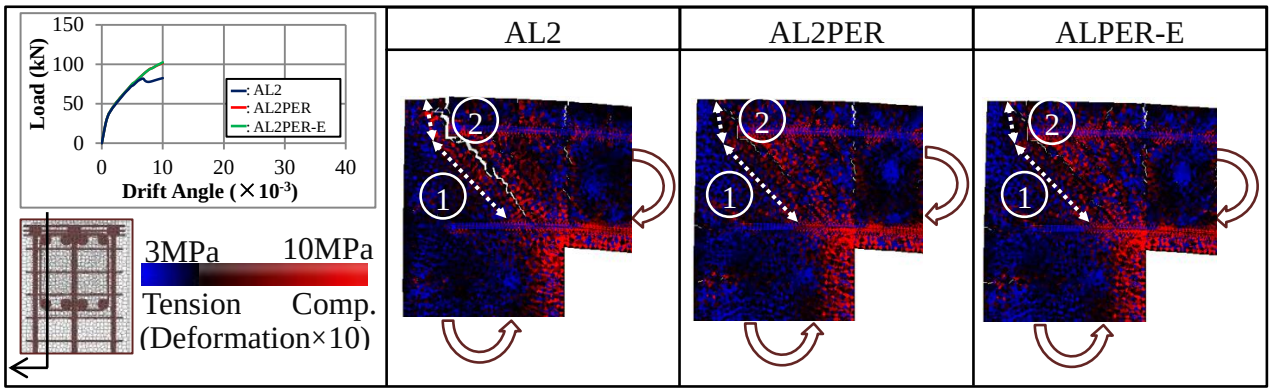

Fig. 11 – Internal stresses for AL2, AL2PER, and AL2PER-E at a drift angle of 10×10^{-3} rad

4.3 Effect of perpendicular beams and failure mode

Figure 11 shows the internal stress distributions in AL2, AL2PER, and AL2PER-E at a drift angle of 0.010 rad, at a cross section where the beam reinforcing bars are present. These internal stress distributions show that bonding is improved in AL2PER and AL2PER-E because of the perpendicular beams. As the drift angle increases, diagonal cracks, propagating from the anchorage plates of the top longitudinal reinforcement in the beam to the inner corner of the beam-column joint, occur in the beam-column joint (1). In AL2PER and AL2PER-E, the occurrence of these diagonal cracks is delayed to a drift angle of around 0.008 rad because of the improved bond performance along the development length of anchorages.

In AL2, these diagonal cracks cause a slight drop in the load at a drift angle of around 0.007 rad as illustrated in Fig. 8(b). Meanwhile, in AL2PER and AL2PER-E, the load does not drop because the opening of the diagonal cracks is smaller than AL2. As the drift angle increases, cracks propagate behind the anchorage plates because the interface between anchorage plates and concrete is weak in tension. These cracks and diagonal cracks join together and penetrate to the top surface of the joint (2). As a result, when diagonal cracks open wider, cracks behind the anchorage plates also open wider.

Figure 12 shows the internal stress distributions in AL2, AL2PER, and AL2PER-E at a drift angle of 0.020 rad, at a cross section where the beam reinforcing bars are present. As the drift angle increases, diagonal cracks open.

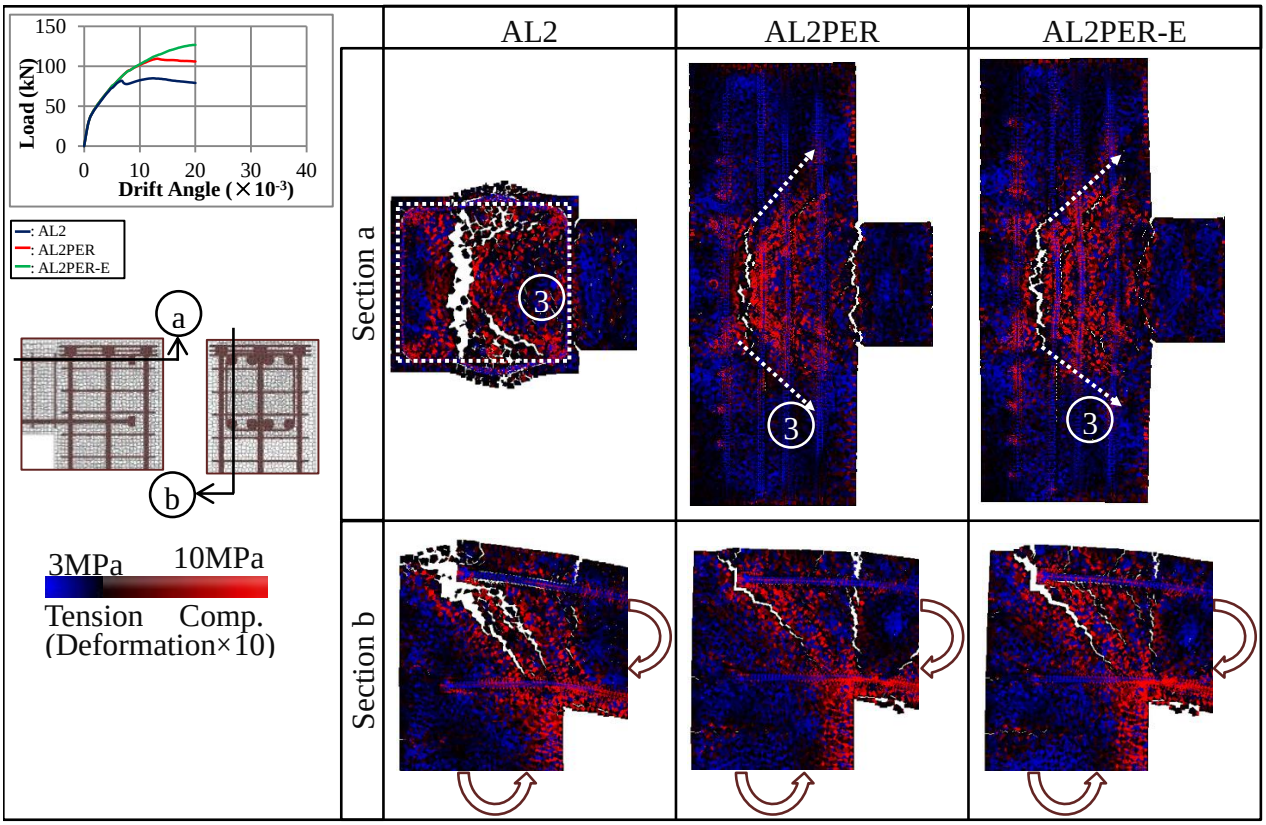

Fig. 12 – Internal stresses for AL2, AL2PER, and AL2PER-E at a drift angle of 20×10^{-3} rad

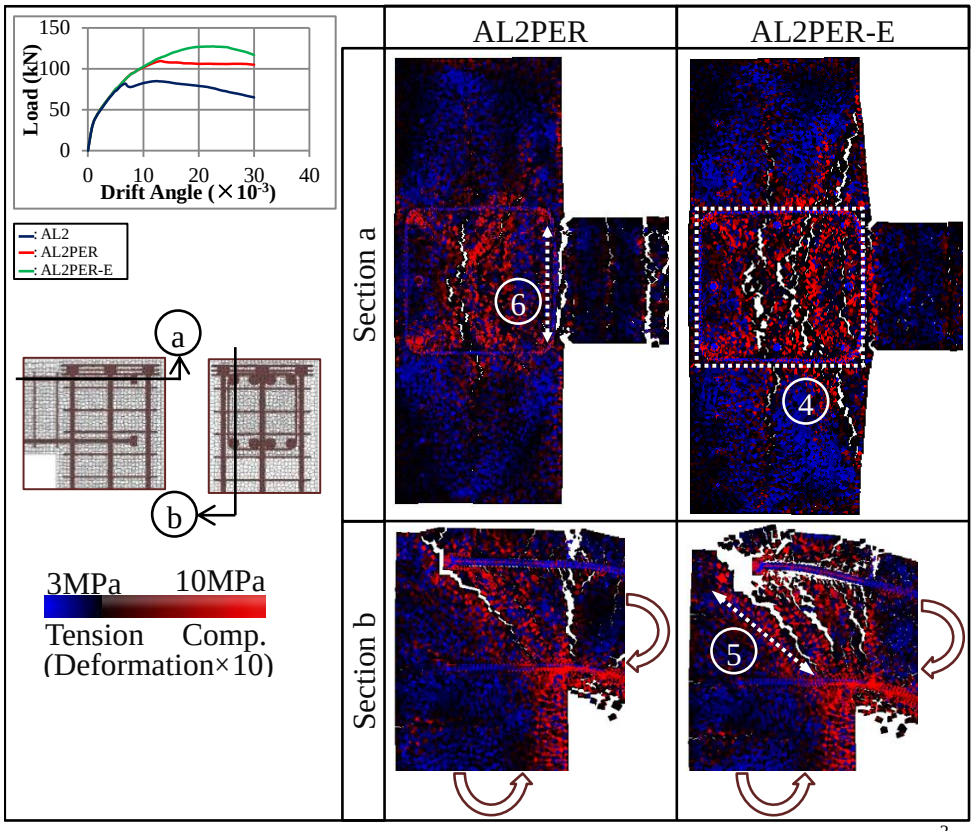

Fig. 13 – Internal stresses for AL2PER and AL2PER-E at a drift angle of 30×10^{-3} rad

In AL2, the damage at the top surface of the joint occurs which indicates the anchorage failure (3). Furthermore, diagonal cracks open easily, so there is a significant drop in the loading capacity after the maximum load. In AL2PER and AL2PER-E, as the diagonal cracks open, stresses spread out to the perpendicular beams (3). These stresses resist the opening of the diagonal cracks and a diagonal compressive strut still forms in the beam-column joint. Ultimately, the flexural failure occurs and the load does not decrease beyond the maximum load in AL2PER. Through the study of the internal stresses and internal cracks in the numerical models, it is clarified that the perpendicular beams increase the bond performance and resist the opening of diagonal cracks.

Figure 13 shows the internal stress distributions in AL2PER and AL2PER-E at a drift angle of 0.030 rad, at a cross section where the beam reinforcing bars are present. In AL2PER-E, as the drift angle increases, the damage at the top surface of the joint occurs which indicates the anchorage failure (4). As the damage occurs at the top surface of the joint, diagonal cracks open easily (5) and, furthermore, the load decreases significantly once the maximum load is exceeded. As mentioned above, it has the same failure mode as that in AL2, but the occurrence of the anchorage failure is delayed in AL2PER-E. In AL2PER, flexural cracks are wider because of the flexural failure (6).

Figure 14 shows the internal stress distribution in AL2PER-E at a drift angle of 0.040 rad, at a cross section where the beam reinforcing bars are present. Local stresses are generated only up to a certain length of the perpendicular beams called the effective length. It is proposed by the simulation that the effective length of the perpendicular beams is determined by approximately 45 degrees inclination to the longitudinal beam, measured from the original position of anchorage plates.

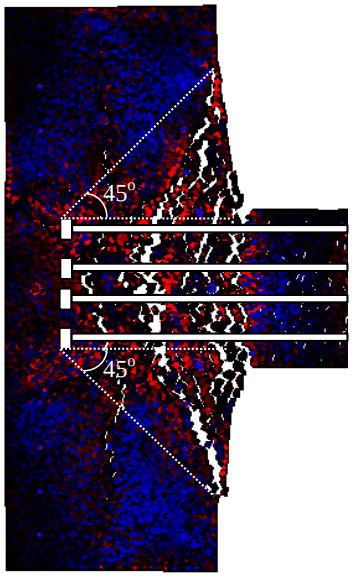

Fig. 14 – Internal stresses for AL2PER-E at a drift angle of 40×10^{-3} rad

5. Conclusions

Based on the study of the effect of perpendicular beams on the failure of a beam-column knee joint with mechanical anchorages using 3D RBSM meso-scale simulations, the following conclusions can be drawn.

(1) The simulations of the beam-column knee joints with mechanical anchorages give good predictions in terms of load-displacement relationships and surface cracks. The simulation also captures the failure behavior seen in the experiment, in which an anchorage failure occurs in AL2. Based on the simulation results, perpendicular beams improve the performance of a beam-column knee joint with mechanical anchorages in terms of the loading capacity and the failure behavior. In AL2PER, the loading capacity is increased by 28.8%, and furthermore a flexural failure occurs in this case. In AL2PER-E, the loading capacity is increased by 49.9%, but an anchorage failure occurs in this case.

(2) Through a study of the internal stresses and cracks modelled by 3D RBSM, it is proposed that the perpendicular beams have two effects. They improve bonding along the development length of the anchorages and resist the opening of diagonal cracks. As diagonal cracks open, stresses spread out to the perpendicular beams and resist the opening of diagonal cracks.

(3) The failure mode of a beam-column knee joint with mechanical anchorages when perpendicular beams are added on both sides of the joint is revealed by the simulation results. It has the same failure behavior as in the case without perpendicular beams which is an anchorage failure, but the occurrence of the anchorage failure is delayed in the case with perpendicular beams. It is also proposed by the simulation that the effective length of the perpendicular beams is determined by approximately 45 degrees inclination to the longitudinal beam, measured from the original position of anchorage plates.

References

1. Wallace, J. W.; McConnel, S. W.; Gupta, P.; and Cote, P. A. (1998) "Use of headed reinforcement in beam-column joints subjected to earthquake load," ACI Structural Journal, 95(5), pp. 590~606.
2. Chun, S. C.; Lee, S. H.; Kang, T. H. K.; and Wallace, J. W. (2007) "Mechanical anchorage in exterior beam-column joints subjected to cyclic loading," ACI Structural Journal, 104(1), pp. 102~112.
3. Tasai, A.; Kusunoki, K.; Kiyohara, T.; and Adachi, T. (2012) "Structural performance of reinforced concrete roof exterior beam column joint with headed bars," Proceedings of the 15th World Conference on Earthquake Engineering, Lisboa.
4. Suzuki, A.; Gotoh, Y.; Tasai, A; and Kusunoki, K. (2012) "Experimental study on the hysteric characteristics of the RC T-shape beam-column joint using mechanical anchorage," Proceedings of Japan Concrete Institute, 31(2). (*in Japanese*)
5. Bolander, J. E. and Saito, S. (1998) "Fracture analysis using spring networks with random geometry," Engineering Fracture Mechanics, 61(5), pp. 569~591.
6. Bolander, J. E.; Yoshitake, K.; and Thomure, J. (1999) "Stress analysis using elastically homogeneous rigid-body-spring networks," Journal of Japan Society of Civil Engineers, 633, pp. 25~32.
7. Bolander, J. E. and Le, B. D. (1999) "Modeling crack development in reinforced concrete structures under service loading," Construction and Building Materials, 13(1), pp. 23~31.
8. Bolander, J. E.; Hong, G. S.; and Yoshitake, K. (2000) "Structural concrete analysis using rigid-body-spring networks," Computer-Aided Civil and Infrastructure Engineering, 15(2), pp. 120~133.
9. Bolander, J. E. and Hong, G. S. (2002) "Rigid-body-spring network modeling of prestressed concrete members," ACI Structural Journal, 99(5), pp. 595~604.
10. Bolander, J. E.; Choi, S.; and Duddukuri, S. R. (2008) "Fracture of fiber-reinforced cement composites: effect of fiber dispersion," International Journal of Fracture, 154(1-2), pp. 73~86.
11. Nam, J. W.; Abell, M. P.; Lim, Y. M.; and Bolander, J. E. (2010) "Strength degradation of fiber-reinforced cement composites exposed to simulated environments," ACI Special Publications, 272.
12. Bolander, J. E. and Berton, S. (2004) "Simulation of shrinkage induced cracking in cement composite overlays," Cement and Concrete Composites, 26(7), pp. 861~871.
13. Wang, T.; Eddy, L.; and Nagai, K. (2014) "Numerical simulation of failure of beam column joint with mechanical anchorage by 3D discrete analysis," Proceedings of the 6th Asia Pacific Young Researchers and Graduates Symposium, Bangkok, Thailand.
14. Nagai, K.; Hayashi, D; and Eddy, L. (2014) "Numerical simulation of failure of anchorage with shifted mechanical anchorage bars by 3D discrete model," Advances in Structural Engineering, 17(6), pp. 861~870.
15. Kawai, T. (1978) "New discrete models and their application to seismic response analysis of structures," Nuclear Engineering and Design, 48(1), pp. 207~229.
16. Nagai, K.; Sato, Y.; and Ueda, T. (2005) "Mesoscopic simulation of failure of mortar and concrete by 3D RBSM," Journal of Advanced Concrete Technology, 3(3), pp. 385~402.
17. Shima, H.; Chou, L. L.; and Okamura, H. (1987) "Micro and macro models for bond in reinforced

concrete," Journal of Faculty of Engineering, The University of Tokyo, 39(2), pp. 133~194.
18. Architectural Institute of Japan. (2010). "AIJ Standard for Structural Calculation of Reinforced Concrete Structures". (*in Japanese*)

Notation

b_j : effective width of beam-column joint (mm)
D_j : column depth (mm)
E_c : modulus elasticity of concrete (MPa)
f'_c : compressive strength of concrete (MPa)
f_t : tensile strength of concrete (MPa)
f_{telem} : tensile strength of concrete elements (MPa)
f_y : yield strength of steel bars (MPa)
f_u : tensile strength of steel bars (MPa)
k : $0.032(400/f_y)^{1/3}$
k_j : 0.4
ratio : reduction ratio for normal stress and shear stress
V_{ju} : joint shear strength (kN)
w : crack width between two rigid bodies (mm)
w_{max} : maximum crack width between two rigid bodies (mm)
ε : normal strain of concrete elements (MPa)
ε_s : steel strain
ε_{sh} : initial strain hardening, assumed to be 1.5%
γ : shear strain of concrete elements
ϕ : 0.85
σ : normal stress of concrete elements (MPa)
σ_s : steel stress (MPa)
τ : shear stress of concrete elements (MPa)
τ_{max} : maximum value of shear stress of concrete elements (MPa)